Rheology and Structures of Aqueous Gels of Triblock(oxyethylene/oxybutylene/oxyethylene) Copolymers with Lengthy Oxyethylene Blocks

Antonis Kelarakis,[†] Valeria Castelletto,[‡] Chiraphon Chaibundit,[§] Johan Fundin,[‡] Vasiliki Havredaki,[†] Ian W. Hamley,[‡] and Colin Booth*[,§]

National and Kapodistrian University of Athens, Department of Chemistry, Physical Chemistry Laboratory, Panepistimiopolis, 157 71 Athens, Greece, School of Chemistry, University of Leeds, Leeds LS2 9JT, United Kingdom, and Department of Chemistry, University of Manchester, Manchester M13 9PL, United Kingdom

Received February 5, 2001. In Final Form: April 14, 2001

Four EBE copolymers (E = oxyethylene repeat unit, B = oxybutylene repeat unit) based on a B_{20} central block and end blocks ranging from 58 to 260 E units were studied. Rheological measurements (oscillatory and steady shear) were used to confirm gel boundaries (previously explored by a tube inversion method) and to determine storage and loss moduli (G' and G'') and yield stresses (σ_y) for aqueous gels formed at copolymer concentrations below 20 wt %. The phase diagrams contained a region of hard gel ($G' > G''$, high G' and σ_y), an extensive region of soft gel (($G' > G''$, low G' and σ_y), denoted 1, and a second region of soft gel at low temperatures, denoted 2. Small-angle X-ray scattering was used to probe the hard gel structure. Concentrated aqueous gels (20 wt %) had a body-centered cubic (bcc, $Im\bar{3}m$) structure. The structure of dilute gels near to the hard gel boundary was not defined, although the $Im\bar{3}m$ and $Pm\bar{3}n$ cubic structures were eliminated. Depending on concentration, the soft gels were assigned either to percolation-induced fractal structures (soft gel 1) or to defective cubic structures (soft gels 1 and 2).

1. Introduction

A block copolymer of poly(oxyethylene) and a hydrophobic poly(oxyalkylene) in dilute aqueous solution may form micelles, and its more concentrated micellar solutions will form liquid-crystal mesophases (gels). The most familiar copolymers of this type are the $E_mP_nE_m$ triblocks, where we use E to denote an oxyethylene unit, OCH_2CH_2, and P to denote an oxypropylene unit, $OCH_2CH(CH_3)$, and n and m denote number-average block lengths in repeat units. These copolymers are available from a number of commercial sources, and the phase behaviors, structures, and rheological properties of their gels have been researched in recent years.[1−4]

Aqueous gels of block copolymers of ethylene oxide and 1,2-butylene oxide have also been investigated. We use B to denote the oxybutylene chain unit, $OCH_2CH(C_2H_5)$. A range of E_mB_n and $E_mB_nE_m$ copolymers is available from The Dow Chemical Co.,[5] but many more have been synthesized in Manchester.[6,7] Recent work has been concentrated on aqueous gels of diblock E_mB_n copolymers; see refs 8−11 and citations therein. Less attention has been paid to aqueous gels of triblock $E_mB_nE_m$ copolymers. Tube inversion has been used to outline the region of immobile (hard) gel in the phase diagrams of copolymers with lengthy E-blocks ($>E_{40}$) at moderate concentrations,[12−17] and ^{1}H NMR relaxation has been used to confirm the same gel boundaries via changes in the slow correlation time originating from the large-scale motions of the E-blocks.[18] A structural study included 30 and 45 wt % aqueous gels of copolymer $E_{103}B_{15}E_{103}$ at 25 °C, which were shown by small-angle X-ray scattering (SAXS) to have the body-centered cubic (bcc) structure, assumed to be of packed spherical micelles.[17] The application of shear reported for these gels was only to orientate specimens for detailed study by SAXS. The similar shape of the mobile−immobile boundary in all these systems (the same as the boundaries presented in this paper), as well as their isotropy when examined by polarized light micros-

[†] National and Kapodistrian University of Athens.

[‡] University of Leeds.

[§] University of Manchester.

(1) *Nonionic Surfactants*: *Polyoxyalkylene Block Copolymers*; Nace, V. M., Ed.; Surfactant Science Series; Marcel Dekker: New York, 1996; Vol. 60.

(2) Hamley, I. W. *The Physics of Block Copolymers*; Oxford University Press: New York, 1998; Chapter 4.

(3) Reviews in *Amphiphilic Block Copolymers*: *Self-Assembly and Applications*; Alexandridis, P., Lindman, B., Eds.; Elsevier Science B.V: Amsterdam, 2000.

(4) Almgren, M.; Brown, W.; Hvidt, S. *Colloid Polym. Sci.* **1995**, *273*, 2.

(5) *Technical Literature, B-Series Polyglycols. Butylene Oxide/Ethylene Oxide Block Copolymers*; Dow Chemical Co.: Freeport, TX, 1992.

(6) Booth, C.; Attwood, D. *Macromol. Rapid Commun.* **2000**, *21*, 501.

(7) Booth, C.; Yu, G.-E.; Nace, V. M. In *Amphiphilic Block Copolymers*: *Self-Assembly and Applications*; Alexandridis, P., Lindman, B., Eds.; Elsevier Science B.V: Amsterdam, 2000; p 57.

(8) Derici, L.; Ledger, S.; Mai, S.-M.; Booth, C.; Hamley, I. W.; Pedersen, J. S. *Phys. Chem. Chem. Phys.* **1999**, *1*, 2773.

(9) Hamley, I. W.; Daniel, C.; Mingvanish, W.; Mai, S.-M.; Booth, C.; Messe, L.; Ryan, A. J. *Langmuir* **2000**, *16*, 2508.

(10) Kelarakis, A.; Havredaki, V.; Mingvanish, W.; Li, H.; Booth, C.; Daniel, C.; Hamley, I. W.; Ryan, A. J. *Phys. Chem. Chem. Phys.* **2000**, *2*, 2755.

(11) Alexandridis, P.; Olsson, U.; Lindman, B. *Langmuir* **1997**, *13*, 23.

(12) Luo, Y.-Z.; Nicholas, C. V.; Attwood, D.; Collett, J. H.; Price, C.; Booth, C. *Colloid Polym. Sci.* **1992**, *270*, 1094.

(13) Nicholas, C. V.; Luo, Y.-Z.; Deng, N.-J.; Attwood, D.; Collett, J. H.; Price, C.; Booth, C. *Polymer* **1993**, *34*, 138.

(14) Luo, Y.-Z.; Nicholas, C. V.; Heatley, F.; Attwood, D.; Collett, J. H.; Price, C.; Booth, C.; Chu, B.; Zhou, Z.-K. *J. Chem. Soc., Faraday Trans.* **1993**, *89*, 539.

(15) Yang, Z.; Pickard, S.; Deng, N.-J.; Barlow, R. J.; Attwood, D.; Booth, C. *Macromolecules* **1994**, *27*, 2371.

(16) Yang, Y.-W.; Ali-Adib, Z.; McKeown, N. B.; Ryan, A. J.; Attwood, D.; Booth, C. *Langmuir* **1997**, *13*, 1860.

(17) Kelarakis, A.; Havredaki, V.; Derici, L.; Yu, G.-E.; Booth, C.; Hamley, I. W. *J. Chem. Soc., Faraday Trans.* **1998**, *94*, 3639.

(18) Godward, J.; Heatley, F.; Smith, S.; Tandekaew, S.; Yang, Y.-W.; Booth, C. *J. Chem. Soc., Faraday Trans.* **1995**, *91*, 3461.

10.1021/la0101806 CCC: $20.00 © 2001 American Chemical Society
Published on Web 06/12/2001

Table 1. $E_mB_{20}E_m$ Copolymers in Aqueous Solution: Micellar Properties at 25 °C and Limiting Conditions for Hard Gel Formation[a]

copolymer	N_w	r_t/Å	r_h/Å	c*/wt %	T*/°C
$E_{58}B_{20}E_{58}$	27	74	84	13.3	11
$E_{104}B_{20}E_{104}$	21	90	99	11.0	21
$E_{148}B_{20}E_{148}$	15	97	121	9.9	28
$E_{260}B_{20}E_{260}$	9	102	141	9.0	35

[a] N_w, mass-average association number; r_t and r_h, thermodynamic and hydrodynamic radius, respectively; c* and T*, minimum concentration for hard gel formation and associated temperature. Adapted from ref 21.

copy, allowed them all to be characterized as cubic gels. Rather different phase behavior has been reported for aqueous solutions of $E_mB_nE_m$ copolymers with short E-blocks (E_{16}, E_{21}),[7,19] particularly those of copolymer $E_{16}B_{10}E_{16}$ which first form a birefringent hexagonal phase when concentration is increased to the mobile−immobile boundary. This is as expected in view of the comprehensive studies of the gelation behavior of solutions of the related $E_mP_nE_m$ copolymers by Wanka et al.[20]

Our interest in this work is in the cubic gels and focuses on a series of four triblock $E_mB_nE_m$ copolymers based on a central B_{20} block and with E end blocks in the range E_{58}−E_{260}. The rheology of aqueous solutions of the copolymers over a wide range of concentration and temperature is reported, together with an investigation of the structures of aqueous gels at selected concentrations.

2. Experimental Section

2.1. Preparation, Micellization, and Gelation. The preparation and characterization of the copolymers has been described previously.[21] Gel permeation chromatography (GPC) was used to confirm narrow chain length distributions, the ratio of mass- to number-average molar mass (M_w/M_n) being in the range 1.06−1.08 without correction for instrumental spreading. ^{13}C NMR spectroscopy was used to obtain absolute values of the number-average molar mass, and hence the average molecular formulas, and to confirm block architecture and sample purity.

In that previous work,[21] light scattering was used to confirm micellization in dilute solution (critical micelle concentrations of 0.1 g dm^{-3} or less) and to measure micellar properties. Association numbers (N_w) for solutions at 25 °C are listed in Table 1. The thermodynamic radius from static light scattering (SLS) and the hydrodynamic radius from dynamic light scattering (DLS) for solutions at 25 °C are also listed. The thermodynamic radii relate to hard spheres with excluded volumes equivalent to those of the micelles and were determined using scattering theory for hard spheres to fit the slopes and curvatures of Debye plots of the SLS data.[21] The micelles were small compared to the wavelength of the scattered light, and radii of gyration were not accessible. The hydrodynamic radii relate to hard spheres with equivalent diffusional properties to the micelles and were determined from diffusion constants (from DLS) using the Stokes−Einstein equation.[21] As is usually observed for E/B copolymers,[6] the association numbers increased as temperature was increased, but the radii were only weakly dependent on temperature.[21] Included in Table 1 are the minimum concentrations for formation of an immobile (hard) gel (c*) and the corresponding temperatures (T*) as determined by an inverted-tube test.[21] The form of the phase diagram is discussed in section 3.

2.2. Rheometry. The rheological properties of the samples were determined using a Bohlin CS50 rheometer with water-bath temperature control. Couette geometry (bob, 24.5 mm diameter, 27 mm height; cup, 26.5 mm diameter, 29 mm height) was used for all the samples, with a 2.5 cm^3 sample being added to the cup in the mobile state. A solvent trap maintained a water-saturated atmosphere around the cell, and evaporation was not significant for the temperatures and time scales investigated.

Storage and loss moduli were recorded across the temperature range with the instrument in oscillatory-shear mode, usually at a frequency of 1 Hz but for certain systems across the range 0.1−10 Hz. In this mode, the samples were heated at 1° min^{-1} in the range 5−92 °C. For all measurements, the strain amplitude was low (<0.5%, linear viscoelastic region), thus ensuring that G' and G'' were independent of strain.

Measurements of yield stress and viscosity were made at selected temperatures with the instrument in steady-shear mode. The instrument was programmed to increase the shear stress in a series of logarithmically spaced steps, allowing a maximum of 1 min to equilibrate at each step. Usually, a period of 30 min was allowed for temperature equilibration before starting the program at any given temperature.

2.3. Small-Angle X-ray Scattering. SAXS experiments were conducted at the Synchrotron Radiation Source, Daresbury Laboratory, U.K. Experiments on 20 wt % gels were carried out on beamline 16.1.[22] These gels were subjected to either steady shear or oscillatory shear using a Couette cell described previously.[23] The X-ray beam was in the radial direction, passing through the center of the Couette cell. Thus, SAXS patterns were collected in the (**v**,**e**) plane, where **v** denotes the flow direction and **e** denotes the neutral (vorticity) direction. A water bath[23] enabled investigation of samples under a controlled heating ramp. Experiments on gels with concentrations in the range 10−15 wt % were conducted on station 8.2, details of which are provided elsewhere.[24] Gels were placed into a liquid cell, comprising a brass cell with mica windows and a poly(tetrafluoroethylene) spacer ring. Heating in the brass holder was accomplished using a water bath. The scattering vector used in presentation of results is defined by $q = (4\pi/\lambda) \sin \theta$, where 2θ is the scattering angle and λ is the wavelength (1.5 Å).

3. Results

3.1. Rheological Behavior. Most attention was paid to the two longer copolymers and particularly to copolymer $E_{260}B_{20}E_{260}$. Accordingly, it is convenient to describe the rheology of solutions of that copolymer first.

3.1.1. Copolymer $E_{260}B_{20}E_{260}$. The effect of temperature on the storage modulus (G' measured at 1 Hz) of 3−20 wt % aqueous gels is shown in Figure 1. Gel regions are defined by the temperatures at which the plots touch the baseline or reach an obvious minimum. These phases can be characterized either as hard gels (G' at maximum ≈2.5−11 kPa, Figure 1a) or as soft gels (G' at maximum ≈10−600 Pa, Figure 1b,c). It is convenient to use the terms "hard" and "soft" gel in the manner of Hvidt et al.[4,25,26] The storage moduli of the sol phases (the baselines in Figure 1) were usually 1 Pa or less.

Selected data are replotted as log(modulus) in Figure 2 in order to show the relationship to the parallel definition of gel ($G' > G''$) and sol ($G' < G''$). With only minor exceptions (for example, the 10 wt % solution, Figure 2), this definition gives the same boundary temperatures. These log(G) plots serve to show that the high-T phase is a soft gel and not a sol.

(19) Yu, G.-E.; Li, H.; Fairclough, J. P. A.; Ryan, A. J.; McKeown, N.; Ali-Adib, Z.; Price, C.; Booth, C. *Langmuir* **1998**, *14*, 5782.

(20) Wanka, G.; Hoffmann, H.; Ulbricht, W. *Macromolecules* **1994**, *27*, 4145.

(21) Chaibundit, C.; Mai, S.-M.; Heatley, F.; Booth, C. *Langmuir* **2000**, *16*, 9645.

(22) Bliss, N.; Bordas, J.; Fell, B. D.; Harris, N. W.; Helsby, W. I.; Mant, G. R.; Smith, W. R.; Towns-Andrews, E. *Rev. Sci. Instrum.* **1995**, *66*, 1311.

(23) Pople, J. A.; Hamley, I. W.; Diakun, G. P. *Rev. Sci. Instrum.* **1998**, *69*, 3015.

(24) Bras, W.; Derbyshire, G. E.; Ryan, A. J.; Mant, G. R.; Felton, A.; Lewis, R. A.; Hall, C. J.; Greaves, G. N. *Nucl. Instrum. Methods Phys. Res., Sect. A* **1993**, *326*, 587.

(25) Hvidt, S.; Jørgensen, E. B.; Brown, W.; Schillen, K. *J. Phys. Chem.* **1994**, *98*, 12320.

(26) Jørgensen, E. B.; Hvidt, S.; Brown, W.; Schillen, K. *Macromolecules* **1997**, *30*, 2355.

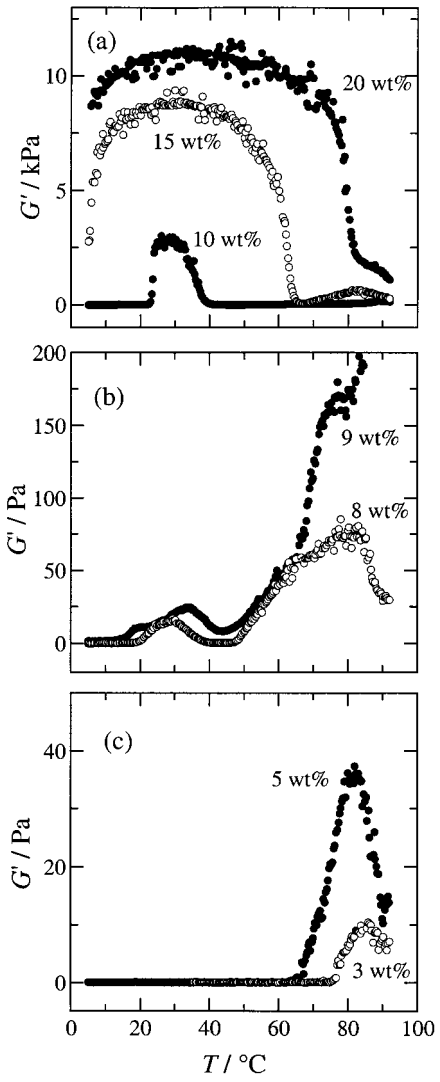

Figure 1. Temperature dependence of dynamic storage modulus ($f = 1$ Hz) for aqueous solutions of block copolymer $E_{260}B_{20}E_{260}$. Copolymer concentrations (wt %) are indicated.

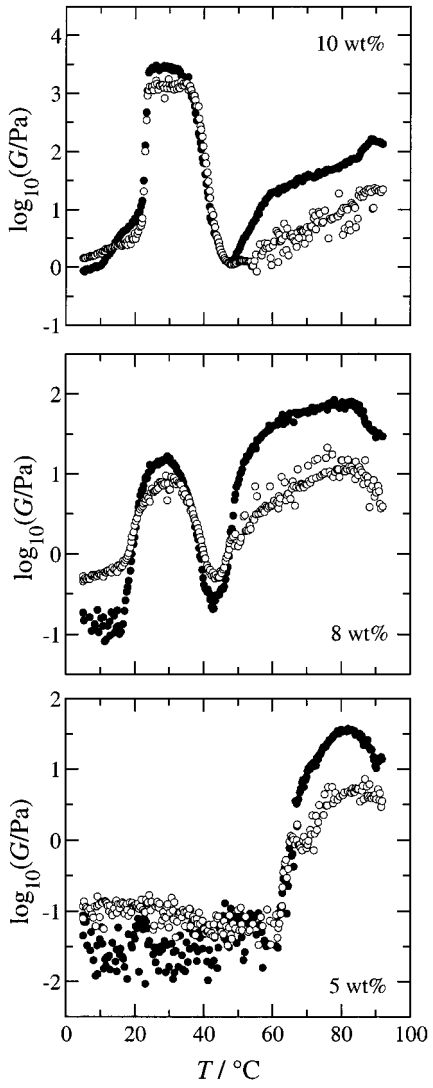

Figure 2. Temperature dependence of logarithmic storage and loss moduli ($f = 1$ Hz) for aqueous solutions of block copolymer $E_{260}B_{20}E_{260}$. Filled symbols denote log(G'), and unfilled symbols denote log(G''). Copolymer concentrations (wt %) are indicated.

The phase boundaries defined in this way are shown in Figure 3, together with the immobile gel boundary obtained by an inverted-tube method (reported previously).[21] The correspondence between the hard gel phase from rheometry and the immobile gel phase from the inverted-tube test is apparent, and the term hard gel can be used irrespective of experimental method. Two soft gel regions are distinguished, denoted 1 and 2.

3.1.2. Copolymers $E_{148}B_{20}E_{148}$, $E_{104}B_{20}E_{104}$ and $E_{58}B_{20}E_{58}$. Results obtained for solutions of copolymer $E_{148}B_{20}E_{148}$ are illustrated in Figures 4 and 5. They are similar to those for corresponding solutions of copolymer $E_{260}B_{20}E_{260}$ (shown in Figures 1 and 2) but differ in one respect: a signal attributable to soft gel 2 is not resolved. However, a feature of the $G(T)$ curves for 9 and 7 wt % solutions of copolymer $E_{148}B_{20}E_{148}$ is a tail on the low-T side of the soft gel peak, and this region is assigned to soft gel 2. Further evidence for a soft gel 2 phase is found in the similarity of the log(G) curves obtained for their 10 wt % solutions (see Figures 2 and 5). Phase boundaries are shown in Figure 6a, where the form of the diagram is similar to that found for solutions of copolymer $E_{260}B_{20}E_{260}$; see Figure 3.

The results found for solutions of copolymer $E_{58}B_{20}E_{58}$ and $E_{104}B_{20}E_{104}$ follow the same pattern; see Figure 6b,c.

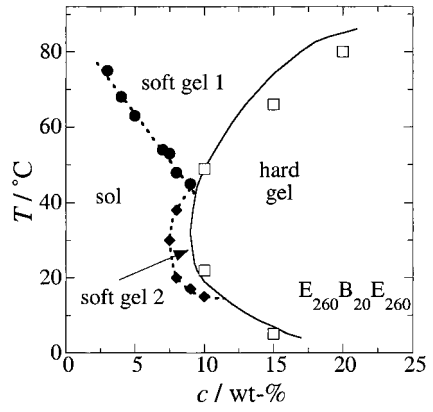

Figure 3. Phase boundaries for aqueous solutions of block copolymers $E_{260}B_{20}E_{260}$. The hard gel boundary (full curve) was established using tube inversion. The unfilled data points (□) derive from oscillatory rheology. The filled data points (●, ◆) and the dashed curves denote the sol/soft gel boundary from rheology.

In particular, low-temperature shoulders to the $G(T)$ plots (see Figure 7 for examples) can be interpreted as evidence of a second soft gel phase. As seen in the figures, the hard

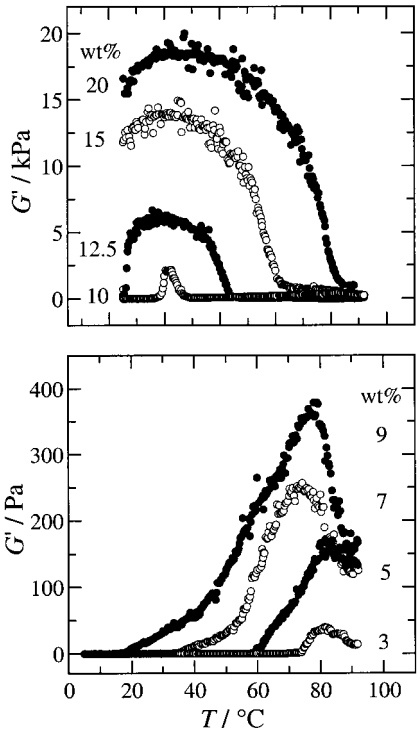

Figure 4. Temperature dependence of dynamic storage modulus ($f = 1$ Hz) for aqueous solutions of block copolymer $E_{148}B_{20}E_{148}$. Copolymer concentrations (wt %) are indicated.

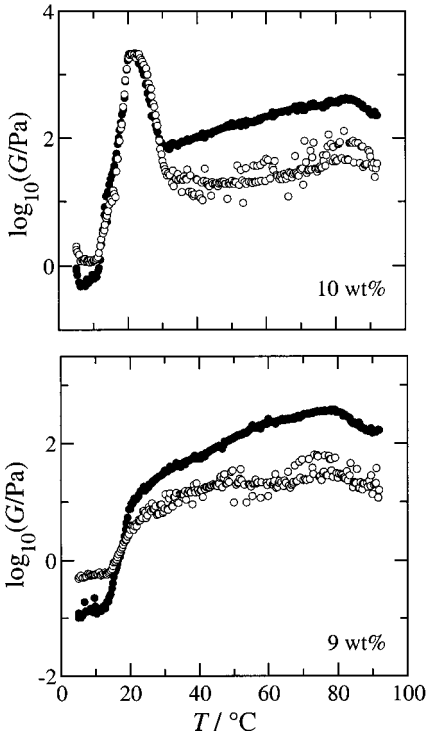

Figure 5. Temperature dependence of logarithmic storage and loss moduli ($f = 1$ Hz) for aqueous solutions of block copolymer $E_{148}B_{20}E_{148}$. Filled symbols denote log(G'), and unfilled symbols denote log(G''). Copolymer concentrations (wt %) are indicated.

gel regions of the phase diagrams for these copolymers were only cursorily investigated by oscillatory rheology.

3.1.3. Effect of Frequency. Frequency scans (0.01−30 Hz) were carried out only for hard gels. The results shown in Figure 8 are typical. Log(G') was constant across the frequency range for concentrated hard gels; the

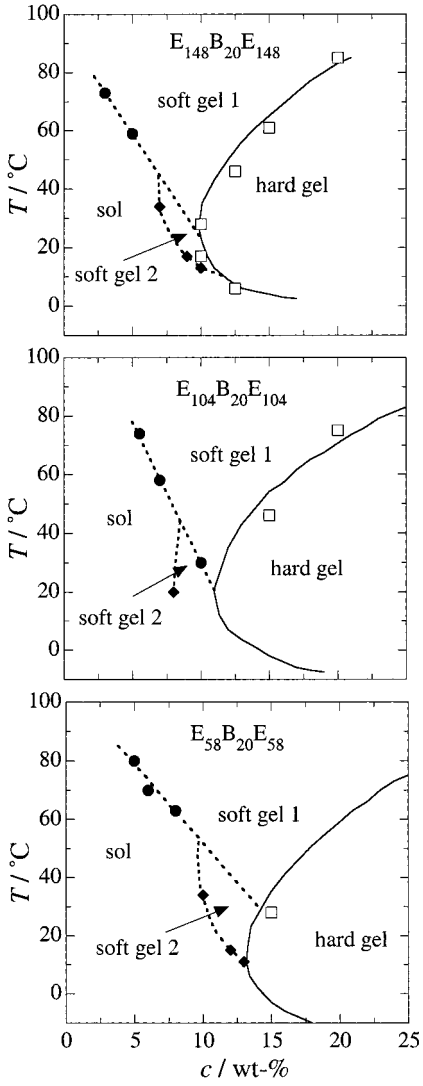

Figure 6. Phase boundaries for aqueous solutions of block copolymers $E_{148}B_{20}E_{148}$, $E_{104}B_{20}E_{104}$, and $E_{58}B_{20}E_{58}$, as indicated. The hard gel boundaries (full curve) were established using tube inversion. The unfilled data points (□) derive from oscillatory rheology. The filled data points (●, ◆) and the dashed curves denote the sol/soft gel boundaries from rheology.

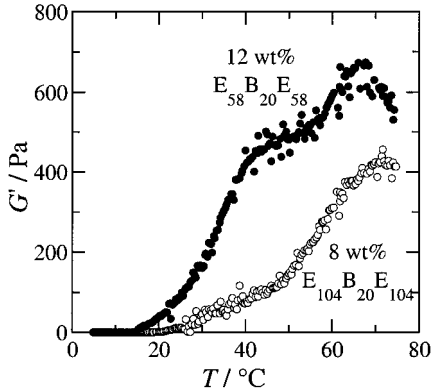

Figure 7. Temperature dependence of dynamic storage modulus ($f = 1$ Hz) for aqueous solutions of block copolymers $E_{104}B_{20}E_{104}$ and $E_{58}B_{20}E_{58}$. Copolymer concentrations (wt %) are indicated.

example in Figure 8 is a 25 wt % gel of copolymer $E_{260}B_{20}E_{260}$ at 25 °C. The loss moduli fell with increasing frequency, as expected for hard gels behaving rheologically

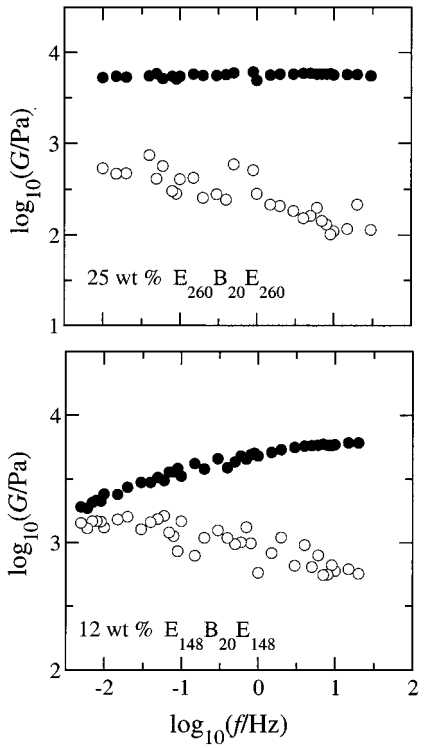

Figure 8. Frequency dependence of storage and loss moduli for aqueous solutions of copolymers $E_{260}B_{20}E_{260}$ (25 wt %) and $E_{148}B_{20}E_{148}$ (12 wt %) at $T = 25$ °C. Filled symbols denote G', and unfilled symbols denote G''.

as a Maxwell element; see Figure 8. For less concentrated hard gels, for example, a 12 wt % gel of copolymer $E_{148}B_{20}E_{148}$ which is near to its critical concentration of $c^* \approx 10$ wt % at 25 °C, G' increased slowly with frequency in the low-frequency range, reaching its plateau value at 1−3 Hz. This insensitivity of storage modulus to frequency, which is expected for a hard gel, meant that the hard gel boundaries defined by rheology were also insensitive to frequency. For the 12 wt % gel of copolymer $E_{148}B_{20}E_{148}$, the crossover of the two moduli was almost reached at the lower limit of our frequency range.

The soft gels were examined at just two frequencies, 1 and 10 Hz. The temperature at the soft gel 1 boundary was reduced when measured at high frequency, falling by about 20 °C. The soft gel 2 region was not investigated in these experiments, and lack of material at the end of the investigation made it impossible to carry out a detailed examination of the soft gel regions of the phase diagram. The synthesis of some of the copolymers will be repeated to allow this work to take place.

3.1.4. Yield Stress. Yield stresses were measured for gels in the concentration range 9−20 wt % and at several temperatures. All gels had a measurable yield stress: those of the hard gels were 100 Pa or more, whereas those of the soft gels, both 1 and 2, were 30 Pa or less. Examples of yield stresses found for solutions of copolymers $E_{58}B_{20}E_{58}$ and $E_{260}B_{20}E_{260}$ are given in Table 2.

3.2. Structures from SAXS. SAXS experiments were carried out on 20 wt % hard gels of all four copolymers at 20 °C. Although two-dimensional diffraction patterns were obtained for orientated samples under shear in the Couette cell, here we focus on data for as-mounted samples in order to compare with domain spacings obtained for unsheared gels of lower concentration (see below). Figure 9 shows the diffraction patterns for the 20 wt % gels reduced to one-dimensional profiles by integration of the

Table 2. Yield Stresses (σ_y) of Aqueous Solutions of Copolymers $E_{58}B_{20}E_{58}$ and $E_{260}B_{20}E_{260}$

copolymer	c/wt %	T/°C	σ_y/Pa	phase[a]
$E_{58}B_{20}E_{58}$	15	5	360	hard
		25	200	hard
		45	5	soft 1
$E_{260}B_{20}E_{260}$	20	5	300	hard
		45	400	hard
		85	150	hard
	9	5	0	sol
		15	0	sol
		25	10	soft 2
		65	4	soft 1
		85	10	soft 1

[a] From Figures 3 and 6.

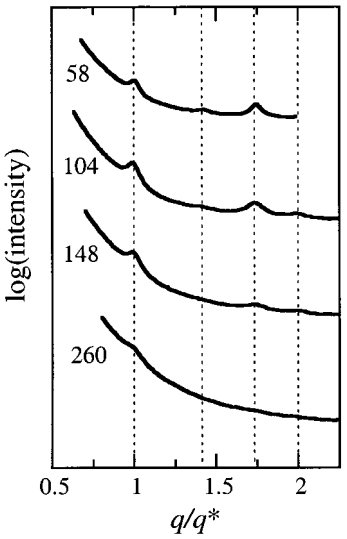

Figure 9. Profiles of intensity versus q/q^* for 20 wt % aqueous gels of $E_mB_{20}E_m$ copolymers, as indicated by the values of m shown. The profiles were obtained by integration of the SAXS patterns obtained using the Couette cell. Spacing $d^* = 2\pi/q^*$ is listed in Table 3. The dashed lines indicate the ratios q/q^* expected for a bcc structure.

two-dimensional pattern. The sequence of reflections obtained for the gels of copolymers $E_{58}B_{20}E_{58}$, $E_{104}B_{20}E_{104}$, and $E_{148}B_{20}E_{148}$ were characteristic of the bcc structure, with reflections at $q/q^* = 1, \sqrt{2}, \sqrt{3}, \sqrt{4}$,..., where q is the scattering vector and q^* is its value at the first-order (110) reflection. The second-order reflection at $\sqrt{3}q^*$ is very weak. The SAXS profile shown for the gel of copolymer $E_{260}B_{20}E_{260}$ gives evidence only of a first-order reflection; see Figure 9. A problem of this type has been encountered previously in assigning the bcc structure to hard gels of diblock copolymers with lengthy E-blocks.[9] As in that case, the two-dimensional patterns obtained from the present samples when orientated in the Couette cell provided confirmatory evidence of the bcc structure for all four 20 wt % EBE gels. The higher order reflections observed for 20 wt % gels of $E_{58}B_{20}E_{58}$ and $E_{104}B_{20}E_{104}$, together with the azimuthal orientation of reflections for these gels and those of the other two copolymers, were consistent with the bcc (space group $Im\bar{3}m$) structure previously identified for gels of EB[8,9,27] and other EBE[17] copolymers.

SAXS was also recorded for copolymer solutions with concentrations some 1−2 wt % higher than the limiting values for hard gel formation (c^*, see Table 1). The SAXS patterns were obtained with a one-dimensional detector

(27) Hamley, I. W.; Pople, J. A.; Fairclough, J. P. A.; Ryan, A. J.; Booth, C.; Yang, Y.-W. *Macromolecules* **1998**, *31*, 3906.

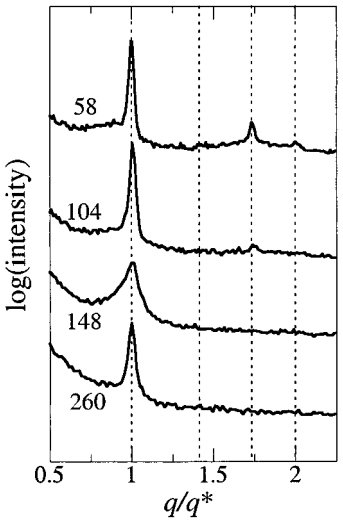

Figure 10. Profiles of intensity versus q/q^* for 11−15 wt % aqueous gels of $E_mB_{20}E_m$ copolymers, as indicated by the values of m shown. The profiles were obtained with the liquid cell and the one-dimensional detector. Spacing $d^* = 2\pi/q^*$ is listed in Table 3. The dashed lines indicate the ratios q/q^* expected for a bcc structure.

using the liquid cell, that is, without shear orientation. Intensity profiles found for hard gels at 25 °C are shown in Figure 10. The marked difference in relative intensities compared with Figure 9 is caused by a combination of effects: different transmission factors for the Couette and liquid cells, different detectors, and different averaging processes. The intensity profile for the 15 wt % gel of copolymer $E_{58}B_{20}E_{58}$ has peaks in ratio $q/q^* = 1, \sqrt{3}, \sqrt{4}$, and that for the 13 wt % gel copolymer $E_{104}B_{20}E_{104}$ shows the first two reflections of that series. Evidence for a reflection at $q/q^* = \sqrt{2}$ is lacking. The profiles for the more dilute gels of the longer copolymers (11.3 wt % for $E_{148}B_{20}E_{148}$ and 11 wt % for $E_{260}B_{20}E_{260}$) show only one reflection. The single narrow peaks in the intensity profiles of the gels indicate ordered phases. The intensity profiles obtained for the soft gels, for example, at 65 °C, contained one broad peak.

The sequence of reflections $q/q^* = 1, \sqrt{3}, \sqrt{4}$ found for the dilute gel of copolymer $E_{58}B_{20}E_{58}$ would normally be assigned to hexagonal packing of cylindrical micelles. However, at a given temperature, the formation of cylindrical micelles at a lower concentration than spherical micelles would be most unusual in systems of this type: see, for example, studies of aqueous solutions of EPE copolymers[20] or CE oligomers ($C = CH_2$).[28] Moreover, observation of the dilute gel by polarized-light microscopy (PLM) showed no birefringence. These points are discussed in section 4.

4. Discussion

4.1. Hard Gels. It has been shown previously[10,21] that the phase diagrams of a series of copolymers based on a given hydrophobe length can be reduced to a single diagram by plotting $T - T^*$ against $c - c^*$. In Figure 11, the data for the present system are plotted in this way, with values of c^* and T^* taken from Table 1. For clarity, data points for soft gel 2 are omitted. On this diagram, the hard gel samples selected for examination by SAXS fall in the range $c - c^* = 1.4-2$ wt % (dilute gels) and 6.7−11 wt % (concentrated gels).

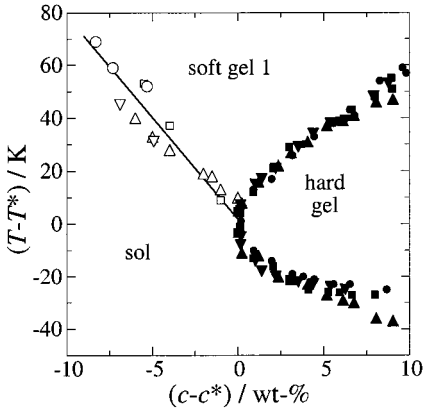

Figure 11. Phase boundaries plotted as $T - T^*$ versus $c - c^*$ for aqueous solutions of $E_mB_{20}E_m$ copolymers: (●, ○) $E_{58}B_{20}E_{58}$, (■, □) $E_{104}B_{20}E_{104}$, (▼, ▽) $E_{148}B_{20}E_{148}$, and (▲, △) $E_{260}B_{20}E_{260}$. c^* is the minimum concentration for hard gel formation, and T^* is the associated temperature.

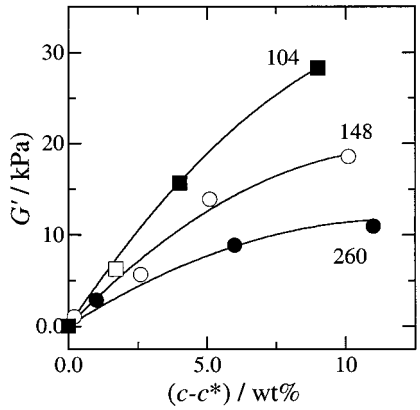

Figure 12. Storage modulus (G', 1 Hz) obtained for hard gels at 25 °C plotted against reduced concentration, $c - c^*$: (●) $E_{260}B_{20}E_{260}$, (○) $E_{148}B_{20}E_{148}$, (■) $E_{104}B_{20}E_{104}$, and (□) $E_{58}B_{20}E_{58}$. c^* is the minimum concentration for hard gel formation.

Values of storage modulus (G', 1 Hz) obtained for the hard gels at 25 °C are plotted against reduced concentration in Figure 12. It is apparent that G' increases as E-block length decreases, as noted previously for diblock EB copolymers.[29] The one data point for copolymer $E_{58}B_{20}E_{58}$ (unfilled square in Figure 12) is not in sequence, but this is remedied if values of G' at T^* are used in the plot, that is, if values corresponding to the maximum in $G'(T)$ are used rather than values at 25 °C. In the regions investigated by SAXS, values of G' at 25 °C range from 3 to 30 kPa; that is, all are stiff gels. The corresponding yield stresses lie in the range 200−300 Pa; see Table 2 for examples.

Domain spacings (d^*) corresponding to the q^* reflection in the SAXS patterns of the EBE copolymer gels (Figures 9 and 10) are plotted as $\log(d^*)$ against $\log(m)$ in Figure 13, where they vary systematically with E-block length (m). From the slopes of the lines in Figure 13, it is found that d^* scales as $m^{0.24\pm0.01}$ (20 wt %) and $m^{0.28\pm0.03}$ (11−15 wt %), very similar scaling relationships one to another and to that found[21] from static light scattering for the thermodynamic radii of micelles of the same copolymers in dilute (<6 wt %) solution, $m^{0.25}$. It is clear that the exclusion properties of the micelle corona scale with E-block length in the same way in the three different environments.

(28) Mitchell, D. J.; Tiddy, G. J. T.; Waring, L.; Bostock, T.; McDonald, M. P. M. *J. Chem. Soc., Faraday Trans. 1* **1983**, *79*, 975.

(29) Kelarakis, A.; Havredaki, V.; Viras, K.; Mingvanish, W.; Heatley, F.; Booth, C. Mai, S.-M. *J. Phys. Chem. B*, accepted.

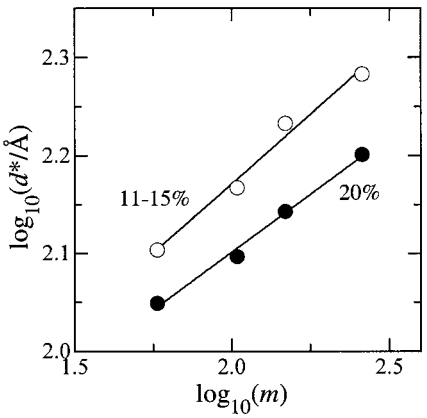

Figure 13. Log−log plot of SAXS domain spacing ($d^* = 2\pi/q^*$) for aqueous hard gels of $E_mB_{20}E_m$ copolymers against E-block length (m): (●) 20 wt % gels and (○) 11−15 wt % gels.

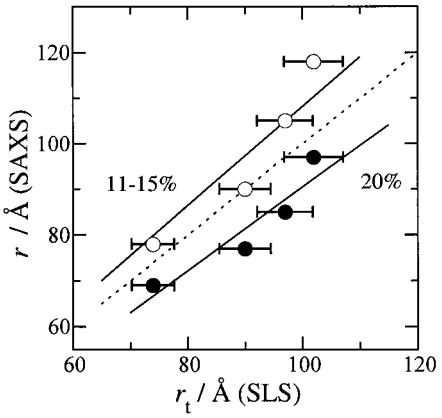

Figure 14. Micelle radii in (●) 20 wt % gels and (○) 11−15 wt % gels determined by SAXS plotted against micelle thermodynamic radii in dilute solution (<6 wt %) determined by SLS. The micelle radii in the gel were calculated for a bcc structure as described in the text. The error bars for r_t from SLS are ±5%; the error in r from SAXS is small. The full lines, which pass through the origin, are calculated by least squares and serve to smooth the data. The dashed line is $r = r_t$.

Given the established bcc structure of the 20 wt % gels and noting that q^* corresponds to the 110 reflection, the domain spacings can be used to calculate micelle radii in the gel. For the 111 direction, that is, for closest approach, the relation is $r_{gel} = \sqrt{3/8}d^*$. In Figure 14, values of r_{gel} for the 20 wt % gels are plotted (filled circles) against the thermodynamic radii (r_t) of the copolymer micelles measured in dilute solution (see Table 1). Both these radii relate to the exclusion properties of the micelles under equilibrium conditions, that is, to the volume excluded by one micelle to other colliding micelles in the sol state or to contacting micelles in the gel state. The error of determination of r_t is estimated as ±5 Å,[21] as indicated by the error bars in Figure 14. Comparison of the full line with the dotted line ($r = r_t$) shows that values of r_{gel} are lower than those of r_t by 10%, consistent with considerable interpenetration of the E-blocks of the micelle corona in the 20 wt % gel. Similar results have been found previously for aqueous solutions and gels of EB and EBE copolymers,[17] and related studies have been made by Mortensen and co-workers for aqueous solutions and gels of EPE copolymers.[30,31]

Table 3. *d-Spacing from SAXS: T = 25 °C**

copolymer	d^*/Å (20 wt %)	d^*/Å (11−15 wt %)
$E_{58}B_{20}E_{58}$	112	127
$E_{104}B_{20}E_{104}$	125	147
$E_{148}B_{20}E_{148}$	139	171
$E_{260}B_{20}E_{260}$	159	192

Because of the larger d^*-spacing in the 11−15 wt % gels (see Table 3), calculation of r_{gel} in the same way (that is, assuming a bcc structure) leads to larger values. These are shown in Figure 14 as unfilled circles, the full line through these points being some 8% higher than the dotted line ($r = r_t$). In fact, the correlation of critical gel concentration with inverse expansion factor described previously for gels of these and related EBE copolymers[21] demands a more tightly packed structure. Given this previous evidence, the bcc structure has to be rejected for the dilute gels in favor of one with tighter packing. As described above, the SAXS patterns favor a hexagonal structure, and the PLM observations favor an isotropic gel.

The assignment to a hexagonal structure derives essentially from the absence of a SAXS reflection at $q = q^*\sqrt{2}$. An absence can be caused by a minimum in the form factor of the micelles at this scattering vector (the reflection is weak in the SAXS patterns obtained from the 20 wt % gels) or by an accidental orientation of the sample when mounting in the liquid cell such that the $q^*\sqrt{2}$ reflection was directed away from the one-dimensional detector. Taking into account the isotropy and also the fact that we find no obvious discontinuity in the concentration dependence of G' (see Figure 12), we lean toward a cubic structure formed from elongated micelles. Previously,[21] we have speculated that hard gels with concentrations near to c^* might have the cubic structure with eight elongated micelles per unit cell (space group $Pm\bar{3}n$) which has been well documented for micellar solutions by Fontell.[32] However, this structure is not consistent with the present SAXS results. The sequence of reflections allowed for the $Pm\bar{3}n$ space group is 110, 200, 210, 211, 220, 310, 222, 320, ..., leading to peaks in the sequence 1, $\sqrt{2}$, $\sqrt{5/2}$, $\sqrt{3}$, $\sqrt{4}$, $\sqrt{5}$, $\sqrt{12}$, ... There is no evidence for peaks at $q^*\sqrt{5/2}$ in the SAXS patterns of the dilute gels; therefore, this space group can be discounted. Furthermore, even if it was assumed that the first-order reflection was missing or very weak, as often observed for $Pm\bar{3}n$ micellar structures,[33] the sequence of reflections observed for the dilute $E_{58}B_{20}E_{58}$ and $E_{104}B_{20}E_{104}$ gels is still not consistent with an assignment to this space group.

4.2. Soft Gels. Sol/soft gel/hard gel diagrams of the form summarized in Figure 11 have been found for a number of copolymers in water, for example, diblock copolymers E_mB_{18} (m = 96−398),[10] $B_{20}E_m$ (m = 40−610),[29] and $S_{13}E_{60}$,[34] this last being a diblock copolymer prepared from ethylene oxide and styrene oxide, and related phase diagrams have been obtained for aqueous solutions of shorter copolymers, $E_{41}B_8$ and $E_{22}B_7$.[35−37]

(30) Mortensen, K.; Pedersen, J. S. *Macromolecules* **1993**, *26*, 805.
(31) Mortensen, K.; Brown, W.; Norden, W. *Phys. Rev. Lett.* **1992**, *68*, 2340.
(32) Fontell, K. *Colloid Polym. Sci.* **1990**, *268*, 264.
(33) Li, X.; Kunieda, H. *Langmuir* **2000**, *16*, 10092.
(34) Kelarakis, A.; Havredaki, V.; Rekatas, C.; Mai, S.-M.; Attwood, D.; Booth, C.; Ryan, A. J.; Hamley, I. W.; Martini, L. G. A. *Macromol. Chem. Phys.* **2001**, *202*, 1345.
(35) Li, H.; Yu., G.-E.; Price, C.; Booth, C.; Hecht, E.; Hoffmann, H. *Macromolecules* **1997**, *30*, 1347.
(36) Fairclough, J. P. A.; Ryan, A. J.; Hamley, I. W.; Li, H.; Yu, G.-E.; Booth, C. *Macromolecules* **1999**, *32*, 2058.
(37) Mingvanish, W.; Kelarakis, A.; Mai, S.-M.; Daniel, C.; Yang, Z.; Havredaki, V.; Hamley, I. W.; Ryan, A. J.; Booth, C. *J. Phys. Chem. B* **2000**, *104*, 9788.

The formation of soft gels at concentrations lower than c^* has been ascribed to a percolation mechanism whereby structures of weakly interacting spherical micelles form in the system; the transition from sol to soft gel is assumed to occur when micellar aggregates reach a percolation threshold yielding sufficient structure to cause an increase in modulus and, at a suitable frequency, the dynamic storage modulus to exceed the loss modulus.[10,34−38] This explanation is consistent with the interpretation of results (including small-angle neutron scattering (SANS)) obtained for related fluid phases of aqueous solutions of copolymer $E_{13}P_{30}E_{13}$ (coded L64).[39,40]

Hvidt and co-workers,[4,25,26] who studied solutions of EPE copolymers, have described high-temperature soft gels formed from cylindrical micelles. Similar soft gels formed from cylindrical micelles have been reported for solutions of copolymer $E_{22}B_7$,[37] where they are associated with a high-temperature hexagonal hard gel phase.

A third type of soft gel lies either above or below the hard gel region of the phase diagram. The evidence is that these soft gels have defective structures related to that of the hard gel phase. For example, there is SAXS evidence that soft 28.5 wt % aqueous gels of copolymer $E_{41}B_8$ at temperatures above and below the high-T boundary of the hard gel have defective bcc structures.[36] Similarly, Pople et al.,[41] using SAXS, reported soft gels of copolymer $E_{40}B_{10}$ with defective face-centered cubic (fcc) structures above the high-T hard gel boundary, and Prud'homme et al.,[42] using SANS, reported structured soft gels of copolymer $E_{100}P_{65}E_{100}$ (coded F127) below the low-T hard gel boundary.

A second region of soft gel, denoted 2, is distinguished in the present phase diagrams. This feature is omitted from Figure 11 but included in Figures 3 and 6. A parallel might be drawn with solutions of copolymer $E_{16}B_{10}E_{16}$ investigated by Yu et al.[19] However, in that case the second soft gel region was located below the low-T boundary of the hexagonal hard gel and was assigned to a defective hexagonal structure. This is consistent with the hexagonal phase which is first formed on increasing the concentration of $E_{16}B_{10}E_{16}$. Another soft gel region was located at lower concentrations of $E_{16}B_{10}E_{16}$ ($c < c^*$) and was assigned to aggregation of spherical micelles by a percolation mechanism.[19] Cylindrical micelles are formed below c^*, but only at high temperatures.

Against the background set out above, we assign soft gel 1 at $c < c^*$ to percolation-induced fractal structures and at $c > c^*$ to defective cubic structures. Soft gel 2, at low temperatures, is tentatively assigned to defective cubic structures at all concentrations. At low temperatures water is a better solvent for the E-blocks leading to an expansion of the micelle corona. This will increase the effective volume fraction of micelles in solution. At an appropriate micelle volume fraction, soft gel ($G' > G''$) may formed by defective packing. It follows that an increase in temperature will decrease the effective volume fraction and give either a sol or a soft gel by a percolation mechanism, these resulting from the reduced contribution of steric repulsion to the intermicellar potential as temperature is increased and the micelle corona contracts.

5. Concluding Remarks

A number of conclusions can be drawn from the present results for $E_mB_nE_m$ copolymers of variable E-block length but with a given B-block length.

(i) Phase diagrams can be reduced to a single diagram by plotting $T - T^*$ against $c - c^*$, where c^* is the minimum concentration for hard gel formation and T^* is the corresponding temperature.

(ii) Storage moduli of hard gels determined at given $c - c^*$ decrease systematically with E-block length.

(iii) Domain spacings (d^*) corresponding to the first-order reflection in the SAXS pattern also decrease systematically with E-block length. In this case, the scaling relationship, $d^* \sim m^{0.25}$, is the same as that found for the thermodynamic radius (r_t) measured by SLS in dilute solution.

(iv) At concentrations well in excess of c^*, the hard gel structure is bcc. At concentrations near to c^* the structure differs, but it has not proved possible to assign a structure.

(v) A soft gel region in the phase diagram, denoted soft gel 1, is similar to that found for other diblock and triblock copolymers in aqueous solution. This soft gel is assigned to percolation-induced fractal structures at $c < c^*$ and to defective cubic structures at $c > c^*$.

(vi) A second soft gel region, denoted soft gel 2, which occurs at low temperatures, is assigned to defective cubic structures.

There remains considerable uncertainty in respect of structure and rheology for solutions near to the limiting concentration for hard gel. There are inherent difficulties in the structural investigation by SAXS of gels in this region, the most severe being a lack of contrast compared with that in gels at high concentration. Because of this, as noted in (iv) above, the anomalous structure of the dilute hard gels ($c - c^* = 2$ wt %) has not been resolved. Unfortunately, the amounts of the copolymers available at the conclusion of our experiments were insufficient for re-examination of the dilute gels by SAXS combined with shearing in the Couette cell, which would serve to enhance available information by resolving individual Bragg reflections. As mentioned in section 3.1.3, the synthesis of some of the samples will be repeated, and this should allow us to explore the structures and rheology of dilute hard and soft gels in detail.

Acknowledgment. We thank Dr. F. Heatley and Mr. S. K. Nixon for help with the characterization of the copolymers. V.C. was supported by the EU-TMR network "Complex Architectures in Diblock Based Copolymer Systems". Further support was provided by the Thai Government (for C.C.) and the Erasmus Exchange Program of the European Union (for A.K.). The Engineering and Physical Research Council (U.K.) supported the synthesis of block copolymers through Grant GR/L22645, and JF through Grant GR/M51994.

LA0101806

(38) Winter, H. H.; Mours, M. *Adv. Polym. Sci.* **1997**, *134*, 165.
(39) Lobry, L.; Micali, N.; Mallamace, F.; Liao, C.; Chen, S.-H. *Phys. Rev. E* **1999**, *60*, 7076.
(40) Liu, Y. C.; Chen, S.-H.; Huang, J. S. *Macromolecules* **1998**, *31*, 2236.
(41) Pople, J. A.; Hamley, I. W.; Fairclough, J. P. A.; Ryan, A. J.; Komanschek, B. U.; Gleeson, A. J.; Yu, G.-E.; Booth, C. *Macromolecules* **1997**, *30*, 5721.
(42) Prud'homme, R. K.; Wu, G.; Schneider, D. K. *Langmuir* **1996**, *12*, 4651.